Highly sensitive SERS quantification of organophosphorous chemical warfare agents: a major step towards the real time sensing in the gas phase

Marta Lafuente,[a] Ismael Pellejero,[a,b] Víctor Sebastián,[a,c] Miguel A. Urbiztondo,[d] Reyes Mallada,[a,c] M. Pilar Pina*,[a,c] Jesús Santamaría*,[a,c]

[a]Nanoscience Institute of Aragon, University of Zaragoza, Department of Chemical & Environmental Engineering, Edif. I+D+i, Campus Rio Ebro, C/Mariano Esquillor, s/n, 50018 Zaragoza, Spain.
[b]Institute for Advanced Materials, Public University of Navarre, Edif. Jerónimo de Ayanz, Campus Arrosadia, s/n, 31006 Pamplona-Iruña, Spain.
[c]Networking Research Center on Bioengineering, Biomaterials and Nanomedicine, CIBER-BBN, 28029 Madrid, Spain.
[d]Centro Universitario de la Defensa de Zaragoza, 50090 Zaragoza, Spain.
* Corresponding authors: mapina@unizar.es (M.P.P.) and jesus.santamaria@unizar.es (J.S.)

Keywords: SERS, neurotoxic agents, gas phase, real time detection, sub-ppm limit of detection, facile and reproducible fabrication.

Highlights:

- Simple, reproducible and cost-effective SERS-based sensor

- Real time detection of G-agents surrogate at extremely low concentration in gas phase

- SERS substrates based on Au NPs layers with near optimum inter-particle distances

- Citrate coating acts as an effective concentrator of target molecules

Abstract

A surface-enhanced Raman scattering (SERS)-based sensor was developed for the label-free real-time gas phase detection of dimethyl methylphosphonate (DMMP); a surrogate molecule of the G-series nerve agents which are of particular concern due to its extreme toxicity, persistence and previous deployment. The SERS platform was designed using simple elements (Au nano-particles) coated with a citrate layer, and a self-assembly procedure that yields near- optimum distances among the nanoparticles. The citrate coating acts as an effective trap of the target molecules on the immediate vicinity of the Au nanoparticle surface under ambient conditions by reversible hydrogen bonding type interactions. For the first time, we have been able to detect sub-ppm concentrations of DMMP in gas phase (130 parts-per-billion), as might be found on potential emergency scenarios. The high sensitivity, simple

preparation and reusability of the SERS platforms developed in this work open up the way for immediate detection of chemical warfare agents in realistic scenarios.

1   Introduction.

The G-series nerve agents, i.e. Tabun (GA), Sarin (GB), Soman (GD), are widely recognized as one of the most toxic group of chemical warfare agents (CWA) due to the presence of organophosphorus esters causing systemic effects predominantly on the central nervous system. The potential use of highly volatile Sarin (Propan-2-yl methylphosphonofluoridate) by terrorist groups [1,2] has raised considerable public concerning the last decades. In 1995, the Tokyo subway attack performed with Sarin killed 12 people, severely injured 50 and caused temporary injuries in nearly 5000 others [3]. Subsequently, Sarin has been used as a weapon in the Irak (2004) and Syria (2013, 2017) wars. Sarin acute exposure guideline level (AEGL-3) is 0.064 ppmV for an exposure of 10 min [4], *i.e.* the persons expose above this concentration for this period could experience life-threatening health effects or death.

Nowadays, the competing technologies for the rapid detection of chemical agents in gas phase, based on gas chromatography-mass spectroscopy[5,6] and ion mobility spectrometry [7,8], face severe limitations in terms of specificity, portability, cost and simplicity. In general, first responders (FRs) do not have the necessary equipment to perform a rapid and reliable "on site" diagnosis of the scene when dealing with CWAs threats [9]. In addition, the pressure for a fast identification of potential lethal agents in real operational conditions often comes at the expense of the reliability of detection, leading to false alarms that cause chaos and disruption. The review of existing real cases of CWAs attacks clearly indicates that the consequences of non-accidental releases of harmful volatile substances are strongly dependent on the performance of detection systems. It is therefore of high importance to develop methods for the fast and reliable detection of Sarin and similar gases, in such a way that rapid emergency action can be taken.

Surface Enhanced Raman Scattering (SERS) is one of the leading techniques for label-free ultrasensitive vibrational fingerprinting of a variety of molecular compounds [10,11,12]. In the field of explosives and chemical threat detection [13,14], SERS has been identified as key technology thanks to distinctive features such as: ultrahigh sensitivity, detection from a wide variety of matrices and quantification of multiple species in a single measurement, allowing real time detection in the field. Because of its exceptional attributes, a significant impact on point of use homeland security applications is foreseen.

Surface selectivity is key in SERS as strongly enhanced Raman scattering only occurs in very close vicinity (typically less than 10 nm) of the metal when localized surface plasmon nodes are excited [15]. This is even more important for chemical warfare agents (CWAs) that are regarded as poor Raman scatterers [16] with cross-sections in the range of 10^{-29} cm^{2}sr^{-1}molecule^{-1}. Thus, analyte detection at low concentrations is highly challenging unless some effective form of confinement near the surface can be achieved.

Liquids often provide a suitable medium to concentrate the desired molecules in the vicinity of the metal surface. In fact label-free detection in liquid phase of distilled mustard, Sarin and Tabun [17-19] at trace levels on metallic nanostructures has been successfully demonstrated. Particularly outstanding is the detection of femtomol quantities of nerve gases with SERS substrates consisting of flexible superhydrophobic Au-covered Si nanopillars. Similar substrates were applied for ethanol and acetone vapor sensing although in this case the values obtained for limit of detection (LOD) were much higher, *i.e* 1815 ppmV and 3300 ppmV, respectively [20]. SERS detection of hydrogen cyanide (5 ppmV), was successfully achieved [21] on Au coated Si nano-pillar substrates (400 nm in height, 50 nm wide, 18 pillars·μm^{-2}). As could be expected, surface concentration plays a decisive role. The Au film irreversibly traps HCN through the formation of stable [Au(CN)$_2$]-complexes.

The label free SERS detection of target analytes in the gas phase [22] becomes even more challenging for molecules with a low cross section. SERS detection of dimethyl methylphosphonate (DMMP), a G-agents simulant, was demonstrated two decades ago [23] on roughened silver oxide substrates but detection was carried out upon 40 min exposure time and at a concentration of 1000 ppmV. On the other hand, detection of 5000 ppmV of 2-chloroethyl ethyl sulphide (CEES), simulant for HD mustard, has been reported on bare AgFON substrates upon 24 h exposure time [24]. These authors were able to decrease the time scale for unambiguous detection to 15 min by means of functionalization with SAM layers of decanethiol. The sensitivity improvement was attributed to the more favourable orientation of the CEES molecules on functionalised substrates. A considerable advance towards real-time gas detection was demonstrated with 8 ppmV benzenethiol (CWA precursor) on SERS-active AgFON substrates [25] (200 nm Ag film onto 600 nm Silica nanospheres), thanks to the irreversible chemisorption of benzenethiol through a strong S-Ag bond.

SERS detection at trace concentration levels in gas phase is hampered by the fact that only a few molecules of interest are localized at the enhancing surface. Many strategies address this problem including the above mentioned establishment of chemical bonds with the surface. Sometimes, the sample surface can be cooled to cause condensation on the SERS

substrate [26], although this approach is not feasible for field use where low power consumption and fast detection at ambient conditions are required. Alternatively, the SERS can be functionalized for trapping of target analyte. Typical strategies rely on the use of either capture layers to provide high-affinity binding sites or partition layers with low affinity and rapidly reversible binding sites. Thus, the combination of metal-organic framework (ZIF-8) with SERS active structures has been recently attempted [27, 28] for room temperature detection of VOCs. The experimental results reveal evidence for the favourable but reversible interactions between the aromatic compounds and the MOF surface within the sensing volume of SERS, leading to 540 ppmV as LOD for benzene. Similarly, the continuous monitoring of airborne chemicals has been investigated on metallic substrates coated with different polymeric layers [29-32]. In particular, the presence of hydrophobic thiols promoted the interaction with aromatic compounds resulting in enhanced SERS signals. Similarly, PDMS layers on the metallic surface captured vapor molecules from flowing air, placing them in close proximity to the plasmonic hot spots and thus, the thickness of the PDMS film became a critical factor on detection performance. The sorptive material can also be used as nanoparticle support. Thus, Au nanoparticles formed on reduced graphene oxide were successfully tested for the detection of VOCs biomarkers in exhaled breath [33]. The graphene oxide provided both fluorescence quenching and surface area for sorption of analyte molecules and nanoparticle dispersion [34]. The above overview shows that rapid detection of target molecules at low concentrations in air is still highly challenging, especially if it is to be carried out on recyclable cost-effective SERS substrates [35].

In the present work, highly sensitive SERS quantification of DMMP has been demonstrated on citrate-capped Au nanoparticle monolayers (Scheme 1) at extremely low concentration, *e.g.* part-per billion, in gas phase. To obtain the required surface density and distribution of Au nanoparticles a layer by layer adsorption process was optimized using PDDA as cationic polyelectrolyte. The citrate layer on the Au nanoparticles performed as an effective molecular trap by reversible DMMP adsorption on the vicinity of plasmonic Au NPs allowing continuous operation of the SERS sensing platform.

2 Materials and methods.

2.1 Synthesis of Au NPs.

The citrate capped Au nanoparticles were synthesized with a reaction yield of 97% via a modified version of the Turkevich-Frens method [35-36]. 50 mL of aqueous solution (1.1 mM) of $HAuCl_4$ (50% Au basis) was heated to 70°C under stirring, and then 5 mL of

preheated sodium citrate solution (3.8 mM) was added. The solution was kept at 70°C until a red-wine colour appeared, circa 10 min. Then, the liquid was allowed to cool to room temperature. The synthesis experiments have been performed by the platform of Production of Biomaterials and Nanoparticles of the NANBIOSIS ICTS, more specifically by the Nanoparticle Synthesis Unit of the CIBER in BioEngineering, Biomaterials & Nanomedicine (CIBER-BBN).

2.2 SERS substrates.

Au@citrate NPs were deposited onto polished SiO_2/Si chips (1 cm × 1 cm) (Sil'Tronix 1 μm of wet thermal SiO_2) coated with positively-charged poly(diallyl dimethylammonium) (PDDA, 20 wt. % in H_2O from Sigma-Aldrich). Prior to the PDDA deposition, the SiO_2/Si chips were cleaned with oxygen plasma (0.2 mbar O_2, 100 W, 120 s). The best conditions for plasma treated surfaces involved spin-coating a PDDA solution (0.2% v/v in water) at 3000 rpm. After washing by immersion in deionized water and drying in oven at 110 °C for 1 min, the substrates were incubated in the Au@citrate colloidal suspension (0.19 mg ml^{-1}) at 4 °C for 16 hours then rinsed with deionized water, dried with nitrogen and stored.

2.3 Reference Au coated substrates.

Thin films (9 nm) of Au were prepared by electron beam evaporation (Edwards auto-500, 3·10^{-7} mbar, 75 mA, 5.3 KV) onto Si wafers (double side polished Si wafer (100) from Sil'Tronix). These substrates were used as reference for the calculation of the Enhancement Factor (EF) with rhodamine 6G as probe molecule.

2.4 Raman measurements.

An Alpha 300 Raman spectrometer (WITec) was used with a confocal optical microscope (480 nm as lateral spatial resolution). All the spectra were recorded at room temperature with an excitation wavelength of 785 nm, laser power of 2.5 mW, optical lens ×50, 20 s integration time, and 0.05 MHz as detector horizontal shift, unless otherwise indicated. When specific intensity values are reported, these result from the average of three different measurements on the same substrate.

2.5 Material characterization.

SEM (FEG INSPECT 50) and TEM (FEI Tecnai T20) were used to observe the Au@citrate assemblies on Si substrates and to determine the size distribution and morphology. For the examination of the citrate shell thickness, 50 μL of Au@citrate colloidal nanoparticles were mixed during 1.5 h with the same volume of phosphotungstic acid solution

(7.5% w/v) used as staining agent. The dispersion was centrifuged and washed three times with Milli-Q water and later re-suspended. 10 µL of the resulting nanoparticle suspension was placed on a TEM Formvar Carbon 200 mesh-Cu grid, air dried and analyzed in a TEM FEI TECNAI T20 at 200 kV. Average particle size and hydrodynamic size distributions were determined by DLS with a particle size analyzer at a fixed angle of 90° at room temperature (Zeta Plus, Brookhaven Instruments Corporation, NY). UV−vis spectra were obtained on a UV–vis double beam spectrophotometer Jasco V-670. AFM measurements (Multimode 8 from Veeco-Bruker; tip, OMCL-AC240TN-W2 from OLYMPUS, XY resolution < 20nm) were conducted in tapping mode in air to investigate the topography of the metallic coatings. Surface coverage and roughness were estimated by Gwyddion 2.45 analysis of topography images. FT-IR analysis was carried out with VERTEX 70 equipment with microscope slide MKII Golden Gate ATR from 4000 to 700 cm^{-1}, 256 scan and resolution of 0.05 cm-1 to characterize the P-O---H-hydrogen bond interactions between the PO from DMMP and the citrate capping layer of Au NPs.

3 Results and discussion

3.1 Synthesis and deposition of Au@citrate NPs

The citrate capped Au nanoparticles were synthesized with a reaction yield of 97% via modified version of the Turkevich-Frens method [35-36]. The morphology of the Au@citrate nanoparticles was examined by TEM (Figure 1A and 1B) and the diameter of at least 100 particles from two different batches was determined from TEM images. The size distribution has an average size of 22 ± 9 nm (Figure 1C). The elongation of the particles was typically around 1.22; *i.e.* gold particles can be described as spherical in good approximation. The hydrodynamic size evaluated by Dynamic Light Scattering, 30 nm ± 5 nm (Figure S1), was in agreement with the average size determined from TEM images indicating the presence of individual, non-aggregated particles. The UV spectrum of Au@citrate solution shows the intense absorption line at 528 nm in agreement with theoretical calculations [37]. The reproducibility in the synthesis of Au@citrate NPs is good, as indicated by the regularity of the absorption spectra obtained from six independent experiments (Figure 1D). The citrate layer around the nanoparticles with a thickness of 2-5 nm can be seen in the TEM pictures (Figure 2B) after negative staining with phosphotungstic acid.

SERS substrates were prepared using an electrostatically-driven adsorption technique. This facile and inexpensive process was optimized in terms of spin rate and PDDA concentration (Figure S2) to attain a high-density assembly of negatively-charged Au@citrate

NPs onto the SiO$_2$/Si chips. The amounts of Au@citrate particles on the substrate increases for higher PDDA concentration and lower spin rates. The selected procedure yielded homogeneous monolayer of Au@citrate NPs with a surface density on SiO$_2$/Si chips of 700 NPs/μm^2, *i.e.* a coverage degree around 30 % was estimated by *ImageJ* analysis of SEM micrographs (Figure 2A and Figure 2B). In absence of PDDA intermediate layer, Au@citrate particles are not able to interact with the SiO$_2$/Si substrate, therefore, after the incubation step no gold particles remain on the surface (see Figure S2). The SPR spectrum of Au@citrate NPs transferred to the SiO$_2$/Si surface featured a strong broad band with a maximum at 662 nm (Figure 2C). Compared to the LSPR of Au@citrate nanoparticles in solution, the large shift is attributed to the short-range static dipolar coupling between nanoparticles. AFM measurements were also performed in tapping mode on the SERS substrates exposed to ambient conditions (Figure 2D and Figure 2E) to investigate the topography of the metallic coating. Surface coverage values above 35 % of the flat substrate were estimated by Gwyddion 2.45 analysis of topographical images. The metallic surface roughness was in the order of 7 nm. A similar analysis was conducted on PDDA only coated chips to evaluate the thickness of the cationic intermediate layer: below 1 nm (Figure S3). The attained metallic surface topography will lead to enhanced electromagnetic fields or the so-called hot spots [38].

From the number or particles per surface area and their dimensions a value around 35 nm was calculated as the average distance between the centers of neighboring Au@citrate nanoparticles. This value agrees well with the analysis of the average distances from the SEM pictures, which is on average 30.2 ± 8 nm (N > 300). Thus, under optimized preparation conditions, the surface structure can be schematized as shown in Scheme 2. The distances obtained are in the right order of magnitude to obtain a high effectiveness in SERS measurements, provided that the citrate layer can act, as expected as anchor of DMMP molecules [39].

3.2 Quantification of the SERS Substrate Enhancement Factor

In this work, we have mainly used the SERS Substrates Enhancement Factor definition [40-42] to evaluate the SERS activity of the as prepared substrates. Thus, the EF was calculated, using rhodamine 6G (R6G) as probe molecule, according to the following expression:

$$EF = (I_{SERS}/N_{SERS})/(I_{Ref}/N_{Ref})$$

where I_{SERS} is the average surface-enhanced Raman intensity, N_{SERS} is the average number of molecules probed on the SERS substrate, I_{Ref} is the normal Raman intensity collected from the reference substrate and N_{Ref} is the average number of molecules probed in the scattering volume. The Raman signal of R6G at 1504 cm^{-1} (characteristic for C-C stretching) was used for the calculations. To establish the values for I_{Ref} a SiO$_2$/Si chip was covered with a 9 nm thick gold layer using electron beam evaporation (see Figure S4). All the spectra were recorded using a ×50 objective lens, 785 nm wave length laser with a power of 1 mW, and 1.20 μm as spot diameter.

For the reference substrate, the spectrum is acquired focusing on the center of the liquid droplet (2 μL in volume) of aqueous solution of R6G 10^{-3} M. A Raman Intensity, I_{Ref}, of 6.5 counts/s was measured. The number of R6G molecules within the interaction volume [43], N_{Ref}, calculated from the irradiated area and the laser interaction/probe depth, is 3.41×10^{7} molecules. Likewise, a 2 μL of R6G 1 μM aqueous solution was uniformly spread and dried on our SERS substrate in order to measure the value of I_{SERS} under equivalent conditions (11012 counts s^{-1}). The average SERS substrate enhancement factor characterizes the SER intensity of only the first monolayer (directly on the surface). Thus, the R6G 1 μM aqueous solution ensures that the surface coverage of the SERS substrate, assuming uniform distribution over the whole substrate and a packing density of 5 x 10^5 molecules/μm^2, remains smaller than one monolayer (see Supporting Information for details).The surface area of the dried droplet was 4.52 mm^2 and the number of R6G in the droplet is 1.20×10^{12} molecules. With a laser spot size with diameter 1.2 μm, the surface area probed by the laser was 1.13 μm^2. Accordingly, the EF was about 1.93×10^{5}, similar to those reported for Ag-coated Si nanopillar substrates [43].

EF values could vary significantly depending on the experimental procedure to calculate I_{Raman}, N_{Raman} and N_{SERS} (see Table S1). Some authors use the R6G concentration values, instead of number of R6G molecules within the focal beam diameter, to evaluate EF [44]. Following this approach, the EF was about 1.69×10^{6}. Furthermore, EF also depends on the selected laser line. The maximum SERS intensity is achieved when the LSPR (Localized Surface Plasmon Resonance) strongly enhances both the incident and scattered photon intensities.[45] This phenomenon, occurs when the nanoparticles LSPR is little red shifted with respect to the incident wavelength[45, 46]. In this work, the expected superior SERS performance at shorter wavelength laser has been sacrificed to prevent the citrate layer photodegradation.

3.3 SERS detection of DMMP in Gas Phase

SERS experiments for detection of traces of CWA vapors were carried out with DMMP, often used as a Sarin gas simulant thanks to its chemical structure similarities (Figure S5) and its much lower toxicity. For measuring DMMP in gas phase, the SERS substrate was mounted on a home-made gas chamber (2.7×10^{-2} cm^3) placed at an angle of 90° with respect to the 785 nm laser excitation beam (Figure 3). A nitrogen stream (10 STP cm^3 min^{-1}) containing DMMP was fed to the exposure cell, and SERS measurements were immediately performed without any stabilization period. Thanks to the low dead volume of the chamber and connections, the SERS signals intensities attributed to DMMP molecules were nearly stable less than 100 s after injection (Figure S6). Additional efforts are being devoted to improve response time by proper design of a microfluidic device for gas-solid contact.

The Raman spectral profile (Figure S7) agrees to within a few wave numbers with previous reports [47, 48]. The most intense signal appearing at 715 cm^{-1}, mainly assigned to the P-CH$_3$ stretching, has been used as Raman reference line.

As can be observed in Figure 4 and Table 1, the SERS spectrum of high-density Au@citrate monolayers is clearly modified in presence of DMMP vapor, 2.5 ppmV. The characteristic signature of the target at 708 cm^{-1} (band *g* in Figure 4) rapidly develops upon the connection of the gas stream to the cell. The 788 cm^{-1} Raman line, tentatively assigned to O-P-O stretching overlaps with reported bands for citrate molecules at the surface of colloids [49]. A similar effect is found at 831 cm^{-1}, the main Raman line for citrate appears at 844 cm^{-1}, and is attributed to the C-COO stretching. On the other hand, peaks at 467 cm^{-1}, 492 cm^{-1} and 1220 cm^{-1} respectively, (POCH$_3$, PO$_3$ bending and P=O stretching, bands *a*, *b* and *p* in Figure 4) appear clearly and without interference in the spectrum after DMMP dosing. Citrate and DMMP share the stretching O-CH$_3$ at 1028 cm^{-1} and 1081 cm^{-1}; but at the same wavelength, they also exhibit different vibrational modes: at 877 cm^{-1} C-COO stretching of citrate and CH$_3$ bending of DMMP; and COO bending of citrate and CH$_3$ bending of DMMP at 1162 cm^{-1}.

It is well-known that citrate anions coordinate to the gold metal surface by inner-sphere complexation of carboxylate groups. Recent studies [50] reveal that, in addition to coordinated citrates, there are dangling citrate species that are not in direct contact with the metal surface. The same authors have verified the existence of free hydroxyl group of the adsorbed citrate available for other interactions. FT-IR spectra were collected to investigate on the molecular interaction of DMMP molecules with the metallic surface (Figure 5B). For pure DMMP in liquid phase, the intense characteristic broad band centered at 1242 cm^{-1} is

assigned to P-O stretching mode. After saturation of the Au@citrate coatings with DMMP in vapor phase, the broad P-O stretching band has been red-shifted 1230 cm^{-1}, which is plausible [51] because binding of DMMP molecules to the bridging -OH groups in the Au@citrate NPs could significantly decrease the frequency of the P-O stretching mode. The intense band exhibited at 1259 cm^{-1} matches with the interaction between PO groups of neighbouring molecules. In the higher frequency spectral region, i.e. 3600-2700cm^{-1}, the vibrational modes of isolated hydroxyl groups, registered at 3446 and 3257 cm^{-1} on the raw sodium citrate salt and clearly shifted to 3514, 3396 and 3317 cm^{-1} for DMMP saturated Au@citrate samples, also agrees with the postulated P-O-HO-C hydrogen bonding interactions (Figure 5A). At the same time, we cannot exclude the possibility that some organophosphorus molecules were captured at the expense of ammonium groups of the PDDA polyelectrolyte by electrostatic interactions.

Figure 4 comparatively shows the SERS spectra of DMMP over high density Au@citrate monolayers before and after oxygen plasma treatment (0.2 mbar O$_2$, 50 W, 60 s). These relatively mild plasma conditions were carefully defined to ensure the removal of the exposed organic layers while keeping the integrity of Au nanoparticles and their arrangement on the surface (Figure S8). As can be observed, the intensity of the characteristic DMMP Raman line is negligible on the plasma treated substrates when the citrate coating has been completely removed, clearly pointing out to the pivotal role played by the citrate coating to anchor DMMP. Accordingly, the citrate coating not only seems to exhibit an affinity for DMMP vapors, but also has a SERS spectrum that minimally interferes with the Raman spectrum of the analyte. Additional experiments on commercial Au coated SERStrate® substrates, supplied by SILMECO [43] were performed to corroborate the role of the citrate capping agent (Figure S9).

One of the main limitations of SERS-based detection refers to the effect of the lasers used on the target analytes and on the substrate itself. Photo degradation of the target analyte, or the trapping agent leads to signal decay and lower detection efficiency. This problem can be partially alleviated by reducing the flux of photons to the sample by decreasing the laser power, the acquisition time, or both [46]. Figure 6A depicts the evolution of characteristic SERS intensity of DMMP adsorbed on the Au@citrate as a function of integration time for 2.5 mW and 1 mW of excitation power respectively. It can be observed that, within the time-scale studied, (up to 150 s), no photodegradation effects can be ascertained. On the contrary, a continuous signal intensity enhancement is attained during the measured period. The stability of the interaction can also be assessed from the results of Figure 6B, where the standard

measurement was repeated periodically over a 90 min exposure. Three spectra were collected at each time (at different points on the SERS substrate) and the average value was plotted. It can be seen that the SERS intensity remains almost constant *i.e.* a pseudo-equilibrium is rapidly established between DMMP molecules in gas phase (1.2 ppmV) and those adsorbed on the surface of Au@citrate NPs. Similarly, the SERS activity of a given Au@citrate modified SiO$_2$/Si chip was analyzed upon exposure to consecutive cycles on/off DMMP to evaluate the reusability of the SERS substrate. Each cycle of DMMP consisted in feeding DMMP (adsorption) and sweeping it from the SERS substrate using N$_2$ (desorption). Figure 6D illustrates the evolution of SERS spectra with the number of DMMP adsorption/desorption cycles. An excellent reproducibility is observed, with the registered values for the intensities at 718 cm^{-1} Raman line in the adsorption stage being reproduced in each cycle, with a standard deviation of 4.03%. The desorption stage by N$_2$ sweeping led to a complete regeneration of the metallic surface, *i.e.* the Raman line at 718 cm^{-1} disappeared. In addition, the homogeneity of the SERS substrate, often a major concern on SERS detection, was tested by mapping the response of a representative surface. Figure 6C illustrates the Raman SERS mapping across 1×1 mm^2 Au@citrate modified surface. The excellent homogeneity of the SERS substrate is clearly observed, with the presence of hot-spots easily identified over the whole scanned area. The above results indicate the robustness of the system used to create high-density monolayers with the desired characteristics, and the strength of the citrate interaction with DMMP under the conditions employed in this work, making this SERS platform an excellent candidate for continuous field monitoring of CWAs.

Finally, the ability of the SERS platform to detect DMMP at trace (sub-ppm) concentration levels in the gas phase was tested in specific experiments. This is necessary due to the extremely high toxicity of Sarin gas, for which DMMP is a simulant. A highly sensitive detection is required, but at the same time this must be highly reliable to avoid false alarms and unnecessary emergency actions. Optimized SERS detection is uniquely suited for this task as it combines extreme sensitivity with a direct chemical fingerprint that increases reliability. For these low concentrations the DMMP generator (i.e. permeation tube MT-PD-Experimental (107-100-7845-HE3-C50) purchased to VICI) was no longer valid and it was replaced by Tedlar bags filled with the desired DMMP concentration (from 2.5 ppmV down to 625 ppbV). These were prepared by an accurate injection of the proper DMMP liquid amount followed by homogeneization. In this case, the flue gas was continuously sucked using a micropump (3 STP cm^3 min^{-1}). Figure 7A compares the SERS spectra of DMMP obtained over high density Au@citrate monolayers as a function of DMMP concentration:

from 0 up to 2.5 ppmV. The PC stretching peak of DMMP is clearly distinguished upon DMMP dosing, even at the lowest concentration used (625 ppbV). A moderate shift of the characteristic band is observed as the concentration decreases (from 708 cm^{-1} at 2.5 ppmV to at 720 cm^{-1} at 1.2 ppmV and 625 ppbV, respectively). This is expected since it is well known that SERS spectra of adsorbed molecules could slightly shift as a function of the coverage of the surface due to the specific interactions that enhance particular vibrational modes to different extents [25]. The phenomenon is particularly noticeable on SERS spectra at highly diluted conditions, where specific interactions are no longer average over a larger number of molecules. If we assume that it is only the molecules confined in the hot spots, *i.e.* very close to the metal surface, that produce Raman signal, less than 3 molecules of DMMP (Figure S10) are within the effective enhancement volume [52] for the standard vapor concentration herein studied, 2.5 ppmV. The fact that a measurable SERS signal is obtained even at lower number of gas phase molecules, indicates that a higher surface concentration has been achieved, and proves the effectiveness of the citrate layer as a concentrator of DMMP molecules.

The intensity of the characteristic peak (708 cm^{-1} to 720 cm^{-1}) increases linearly with DMMP concentration (Figure 7B). Under the experimental conditions used, the theoretical limit of detection (LOD) calculated as three times the noise level (obtained from the standard deviation value of the PC stretching line intensity of five independent experiments), is 130 ppbV. This value is well beyond any previously reported limits for real-time detection of airborne CWAs [21-24].

4 Conclusions

In summary, a simple and affordable label-free SERS based sensor has been devised for the highly sensitive quantification of dimethyl methylphosphonate in the gas phase via self-assembled high-density Au@citrate monolayers on SiO$_2$/Si substrates. The citrate coating was instrumental in trapping the desired molecule near the surface of the Au nanoparticles by means of reversible hydrogen bonding interactions. On the other hand, the facile preparation procedure developed in this work yielded homogenous, reproducible and robust SERS substrates with near optimal inter-particle distances that were able to co-localize the SERS hot spots and the target analyte molecules. The SERS activity was demonstrated in real-time detection of DMMP, the commonly used surrogate of G-series nerve agents, at extremely low concentration, e.g. detection limit achieved as low as 130 part-per billion in gas phase. Real-time detection is made possible by the rapid response of the SERS signal to changes in the gas phase concentration within the ppb-ppm range studied. Furthermore, the substrates presented

excellent resistance to photodegradation and were easily and quickly regenerated by simply flushing air at ambient conditions. This approach shows great potential for detection of organophosphorous chemical agents in the field with the advantages of simple operation, low cost, reliability and reusability.

Conflicts of interest:

Authors declare that there are no conflicts of interest.

Acknowledgements:

References:

[1] Available from: http://www.theguardian.com/world/2016/mar/14/syria-chemical-weapons-attacks-almost-1500-killed-report-united-nations. Accessed on December 17.

[2] Available from: http://www.telegraph.co.uk/news/2017/04/04/syria-gas-attack-nine-children-among-least-35-people-reported/ Accessed on December17.

[3] A. E. Smithson, L. Levy, Rethinking the lessons of Tokyo. Ataxia: the chemical and biological terrorism threat and the US response. Washington, DC, The Henry L. Stimson Center (2000), 71-111.

[4]Available from: https://www.epa.gov/aegl/agent-gb-sarin-results-aegl-program. Accessed on December 17.

[5] J. A. Contreras, J. A. Murray, S. E. Tolley, J. L. Oliphant, H. D. Tolley, S. A. Lammert, E.D. Lee, D. W. Later, M. L. Lee, Hand-portable gas chromatograph-toroidal ion trap mass spectrometer (GC-TMS) for detection of hazardous compounds J. Am. Soc. Mass Spectrom. 19 (2008) 1425-1434

[6] P. A. Smith, D. Koch, G. L. Hook, R. P. Erickson, C. R. J. Lepage, H. D. Wyatt, G. Betsinger, B. A. Eckenrode, Detection of gas-phase chemical warfare agents using field-portable gas chromatography–mass spectrometry systems: instrument and sampling strategy considerations, TrAC, Trends Anal. Chem. 23 (2004) 296-306.

[7] S. Zimmermann, S. Barth, W. K. Baether, J. Ringer, Miniaturized Low-Cost Ion Mobility Spectrometer for Fast Detection of Chemical Warfare Agents, Anal. Chem. 80 (2008) 6671-6676.

[8] W. E. Steiner, S. J. Klopsch, W. A. English, B. H. Clowers, H. H. Hill, Detection of a Chemical Warfare Agent Simulant in Various Aerosol Matrixes by Ion Mobility Time-of-Flight Mass Spectrometry, Anal. Chem. 77 (2005) 4792-4799

[9] Available from: http://eur-lex.europa.eu/legal-content/EN/TXT/?qid=1431978313741&uri=CELEX:52009SC0790. Accessed on December 17.

[10] R. A. Alvarez-Puebla, L. M. Liz-Marzán, Traps and cages for universal SERS detection, Chem. Soc. Rev. 41 (2012) 43-51.

[11] B. Sharma, R. R. Frontiera, A.I. Henry, E. Ringe, R. P. Van Duyne, SERS: Materials, applications, and the future, Materials Today 15 (2012) 16-25.

[12] P. A. Mosier-Boss, Review of SERS Substrates for Chemical Sensing, Nanomaterials 7 (2017) 142.

[13] R. S. Golightly, W. E. Doering, M. J. Natan, Surface-Enhanced Raman Spectroscopy and Homeland Security: A Perfect Match? ACS Nano 3 (2009) 2859–2869.

[14] A. Hakonen, P. O. Andersson, M. S. Schmidt, T. Rindzevicius, M. Käll, Explosive and chemical threat detection by surface-enhanced Raman scattering: a review, Anal. Chim. Acta 893 (2015) 1-13.

[15] H. Ko, S. Singamaneni, V. V. Tsukruk, Nanostructured Surfaces and Assemblies as SERS Media, Small 10 (2008) 1576- 1599.

[16] S. D. Christesen, J. P. Jones, J. M. Lochner, A. M. Hyre, Ultraviolet Raman Spectra and Cross-Sections of the G-series Nerve Agents, Appl. Spectrosc. 62 (2008) 1078-1083.

[17] F. Inscore, S. Farquharson, Surface-Enhanced Raman Spectral Analysis of Blister Agents and their Hydrolysis Products. Proc. SPIE 6378, Chemical and Biological Sensors for Industrial and Environmental Monitoring II 2006, 63780X.

[18] F. Inscore, C. Shende, A. Sengupta, S. Farquharson, Water Security: Continuous Monitoring of Water Distribution Systems for Chemical Agents by SERS. in Defense and Security Symposium. 2007. International Society for Optics and Photonics. Volume 6540, article id. 654009

[19] A. Hakonen, T. Rindzevicius, M. S. Schmidt, P. O. Andersson, L. Juhlin, M. Svedendahl, A. Boisen, M. Käll, Detection of nerve gases using surface-enhanced Raman scattering substrates with high droplet adhesion, Nanoscale 8 (2016) 1305-1308.

[20] C. L. Wong, U. Dinish, M. S. Schmidt, M. Olivo, Non-labelling multiplex surface enhanced Raman scattering (SERS) detection of volatile organic compounds (VOCs), Anal. Chim. Acta 844 (2014) 54-60.

[21] R. K. Lauridsen, T. Rindzevicius, S. Molin, H. K. Johansen, R. W. Berg, T. S. Alstrøm, K. Almdal, F. Larsen, M. S. Schmidt, A Boisen, Towards quantitative SERS detection of hydrogen cyanide at ppb level for human breath analysis, Sensing and Bio-Sensing Research 5 (2015) 84-89.

[22] S. Emamian, A. Eshkeiti, B.B Narakathu, S. Guruva R. Avuthu, M.Z. Atashbar, Gravure printed flexible surface enhanced Raman spectroscopy (SERS)substrate for detection of 2,4-dinitrotoluene (DNT) vapor, Sens. Actuator B-Chem. 217 (2015) 129-135.

[23] N. Taranenko, J. P. Alarie, D. L. Stokes, T. J. Vo-Dinh, Surface-Enhanced Raman Detection of Nerve Agent Simulant (DMMP and DIMP) Vapor on Electrochemically Prepared Silver Oxide Substrates, Raman Spectrosc. 27 (1996) 379-384.

[24] D. A. Stuart, K. B. Biggs, R. P. Van Duyne, Surface-enhanced Raman spectroscopy of half-mustard agent, Analyst 131 (2006) 568-572.

[25] K. B. Biggs, J. P. Camden, J. N. Anker, R. P. van Duyne, Surface-Enhanced Raman Spectroscopy of Benzenethiol Adsorbed from the Gas Phase onto Silver Film over Nanosphere Surfaces: Determination of the Sticking Probability and Detection Limit Time, J. Phys. Chem. A 113 (2009) 4581-4586.

[26] P. Mosier-Boss, S. Lieberman, Detection of volatile organic compounds using surface enhanced Raman spectroscopy substrates mounted on a thermoelectric cooler, Anal. Chim. Acta 488 (2003) 15-23.

[27] L. E. Kreno, N. G. Greeneltch, O. K. Farha, J. T. Hupp, R. P. van Duyne, SERS of molecules that do not adsorb on Ag surfaces: a metal–organic framework-based functionalization strategy, Analyst 139 (2014) 4073-4080.

[28] G. Zheng, S. de Marchi, V. López-Puente, K. Sentosun, L. Polavarapu, I. Pérez-Juste, E. H. Hill, S. Bals, L. M. Liz-Marzán, I. Pastoriza-Santos, J. Pérez-Juste, Encapsulation of Single Plasmonic Nanoparticles within ZIF-8 and SERS Analysis of the MOF Flexibility, Small 12 (2016) 3935- 3943.

[29] T. Vo-Dinh, SERS chemical sensors and biosensors: new tools for environmental and biological analysis, Sens. Actuator B-Chem. 29 (1995) 183-189.

[30] T. Vo-Dinh, D. Stokes, Surface-enhanced Raman detection of chemical vapors with the use of personal dosimeters, Field Anal. Chem. Technol. 3, (1999) 346-356.

[31] D. Xia, Q. Guo, M. Ge, Y. Yuan, M. Xu, J. Yao, On-line sensitive detection of aromatic vapor through PDMS/C3H7S-assisted SERS amplification, RSC Adv. 6, (2016) 53289-53295.

[32] C. Qian, Q. Guo, M. Xu, Y. Yuan, J. Yao, Improving the SERS detection sensitivity of aromatic molecules by a PDMS-coated Au nanoparticle monolayer film, RSC Adv. 5 (2015) 53306-53312.

[33] Y. Chen, Y. Zhang, F. Pan, J. Liu, K. Wang, C. Zhang, S. Cheng, L. Lu, W. Zhang, Z Zhang, X. Zhi, Q. Zhang, G. Alfranca, J. M. de la Fuente, D. Chen, D. Cui, Breath Analysis Based on Surface-Enhanced Raman Scattering Sensors Distinguishes Early and Advanced Gastric Cancer Patients from Healthy Persons, ACS Nano 10 (2016) 8169-8179.

[34] W. Xu, N. Mao, J. Zhang, Graphene: A Platform for Surface-Enhanced Raman Spectroscopy, Small 9 (2013) 1206-1224.

[35] J. Kimling, M. Maier, B. Okenve, V. Kotaidis, H. Ballot, A. Plech, Turkevich Method for Gold Nanoparticle Synthesis Revisited, Phys. Chem. B 110 (2006) 15700-15707.

[36] E. Luque-Michel, A. Larrea, C. Lahuerta, V. Sebastian, E. Imbuluzqueta, M. Arruebo, M. J. Blanco-Prieto, J. Santamaría, A simple approach to obtain hybrid Au-loaded polymeric nanoparticles with a tunable metal load, Nanoscale 8 (2016) 6495-6506.

[37] W. Haiss, N. T. Thanh, J. Aveyard, D. G. Fernig, Determination of Size and Concentration of Gold Nanoparticles from UV−Vis Spectra, Anal. Chem. 79 (2007) 4215-4221.

[38] X. Liu, S. Lebedkin, H. Besser, W. Pfleging, S. Prinz, M. Wissmann, P. M. Schwab, I. Nazarenko, M. Guttmann, M. M. Kappes, U. Lemmer, Tailored Surface-Enhanced Raman Nanopillar Arrays Fabricated by Laser-Assisted Replication for Biomolecular Detection Using Organic Semiconductor Lasers, ACS Nano 9 (2014) 260-270.

[39] Y. Wang, Y. Wang, H. Wang, M. Cong, W. Xu, S. Xu, Surface-enhanced Raman scattering on a hierarchical structural Ag nano-crown array in different detection ways, Phys. Chem. Chem. Phys. 17 (2015) 1173-1179.

[40] E. Le Ru, E. Blackie, M. Meyer, P. G. Etchegoin, Surface Enhanced Raman Scattering Enhancement Factors: A Comprehensive Study, J. Phys. Chem. C 111 (2007) 13794-13803.

[41] A. D. McFarland, M. A. Young, J. A. Dieringer, van R. P. Duyne, J. Phys. Chem. B 109 (2005), Wavelength-Scanned Surface-Enhanced Raman Excitation Spectroscopy, 11279-11285.

[42] L. Rodríguez-Lorenzo, R. A. Alvarez-Puebla, I. Pastoriza-Santos, S. Mazzucco, O. Stéphan, M. Kociak, L. M. Liz-Marzán, F. J. García de Abajo, Zeptomol Detection Through Controlled Ultrasensitive Surface-Enhanced Raman Scattering, J. Am. Chem. Soc. 131 (2009) 4616-4618.

[43] M. S. Schmidt, J. Hübner, A. Boisen, Large Area Fabrication of Leaning Silicon Nanopillars for Surface Enhanced Raman Spectroscopy, Adv. Mater. 24 (2012) OP11–OP18.

[44] S. Si, W. Liang, Y. Sun, J. Huang, W. Ma, Z. Liang, Q. Bao, L. Jiang, Facile Fabrication of High-Density Sub-1-nm Gaps from Au Nanoparticle Monolayers as Reproducible SERS Substrates, Adv. Funct. Mater. 26 (2016) 8137-8145.

[45] W. Lee, S. Y. Lee, R. M. Briber, O. Rabin, Self-Assembled SERS Substrates with Tunable Surface Plasmon Resonances, Adv. Funct. Mater. 21 (2011) 3424-3429.

[46] R. A. Alvarez-Puebla, Effects of the Excitation Wavelength on the SERS Spectrum, J. Phys. Chem. Lett. 3 (2012) 857-866.

[47] J.C.S. Costa, R.A. Ando, A.C. Santana, P. Corio, Surface-enhanced Raman spectroscopy studies of organophosphorous model molecules and pesticides, Phys. Chem. Chem. Phys. 14 (2012) 15645-15651.

[48] J. J. Brady, M. E. Farrell, P. M. Pellegrino, Discrimination of chemical warfare simulants via multiplex coherent anti-Stokes Raman scattering and multivariate statistical analysis, Opt. Eng. 53 (2014) 021105-021105.

[49] C. H. Munro, W.E. Smith, M. Garner, J. Clarkson, P.C. White, Characterization of the Surface of a Citrate-Reduced Colloid Optimized for Use as a Substrate for Surface-Enhanced Resonance Raman Scattering, Langmuir 11 (1995) 3712-3720.

[50] J.W. Park, J. S. Shumaker-Parry, Structural Study of Citrate Layers on Gold Nanoparticles: Role of Intermolecular Interactions in Stabilizing Nanoparticles, J. Am. Chem. Soc. 136 (2014) 136, 1907-1921.

[51] L. Bertilsson, I. Engquist, B. Liedberg, Interaction of Dimethyl Methylphosphonate with Alkanethiolate Monolayers Studied by Temperature-Programmed Desorption and Infrared Spectroscopy, J. Phys. Chem. B 101 (1997) 6021-6027.

[52] E. Le Ru, P. Etchegoin, Principles of Surface-Enhanced Raman Spectroscopy and Related Plasmonic Effects; Elsevier: Oxford, UK, 2009.

List of captions:

Scheme 1. Schematic diagram of SERS substrate and overview of the experimental set-up.

Figure 1. TEM images of Au@citrate NPs (A) and visualization of the citrate stabilizing layer (B). Statistical analysis of particle size from TEM images (C). Absorption spectrum of six independent synthesis batch of Au@citrate NPs (D); insert: Au@citrate solution in the UV cuvette.

Figure 2. SEM images of high density Au@citrate monolayer onto SiO2/Si chips prepared by LbL assembly: (A) and (B). (C) Normalized UV-VIS spectrum of Au@citrate monolayer onto SiO2/Si chips. AFM characterization of high-density Au@citrate monolayer onto SiO2/Si chips: 2D (D) and 3D topography views (E).

Scheme 2. Schematic representation of the surface structure of Au@citrate monolayer onto SiO_2/Si

Figure 4. SERS spectra of high-density Au@citrate monolayers deposited on SiO2/Si chips during exposure to N2 (light blue) and to 2.5 ppmV DMMP gas (dark blue). Similar spectra have been recorded on O2 plasma treated samples: N2 (pink) and 2.5 ppmV DMMP gas N2 (red). Arrows point the main vibrational modes of DMMP (assignment described in Table 1).

Table 1. Tentative assignment of the experimental SERS bands for DMMP-Au@citrate species.
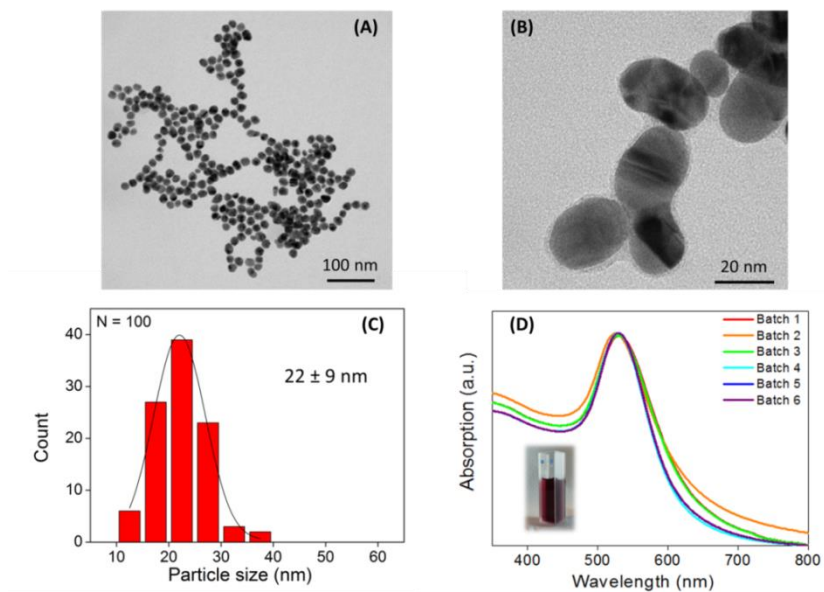
Figure 6. (A) SERS intensity of the Raman line at 718 cm^{-1} as a function of the power at the sample and the integration time in presence of 1.2 ppmV of DMMP in the gas phase. All the measurements were performed on the same chip. (B) SERS intensity values of the Raman lines at 718 cm^{-1} as a function of exposure time to 1.2 ppmV of DMMP in gas phase. All the measurements are performed on the same chip. (C) Raman mapping at 718 cm^{-1} across a 1x1 mm Au@citrate modified SiO_2/Si chip. Conditions: 2.5 mW, 1 s integration time, 1.2 ppmV of DMMP in gas phase and 20 µm as pitch. (D) Evolution of SERS intensity of the Raman line at 718 cm$^-$signal on the SERS substrate exposed to consecutive DMMP adsorption of 1.2 ppmV (green circle) and DMMP desorption in pure N_2 (red circle) cycles.

Figure 7. (A) SERS spectra of high-density Au@citrate monolayers onto SiO_2/Si chips during exposure to pure N_2 and 625 ppbV, 1.2 ppmV and 2.5 ppmV DMMP in gas.
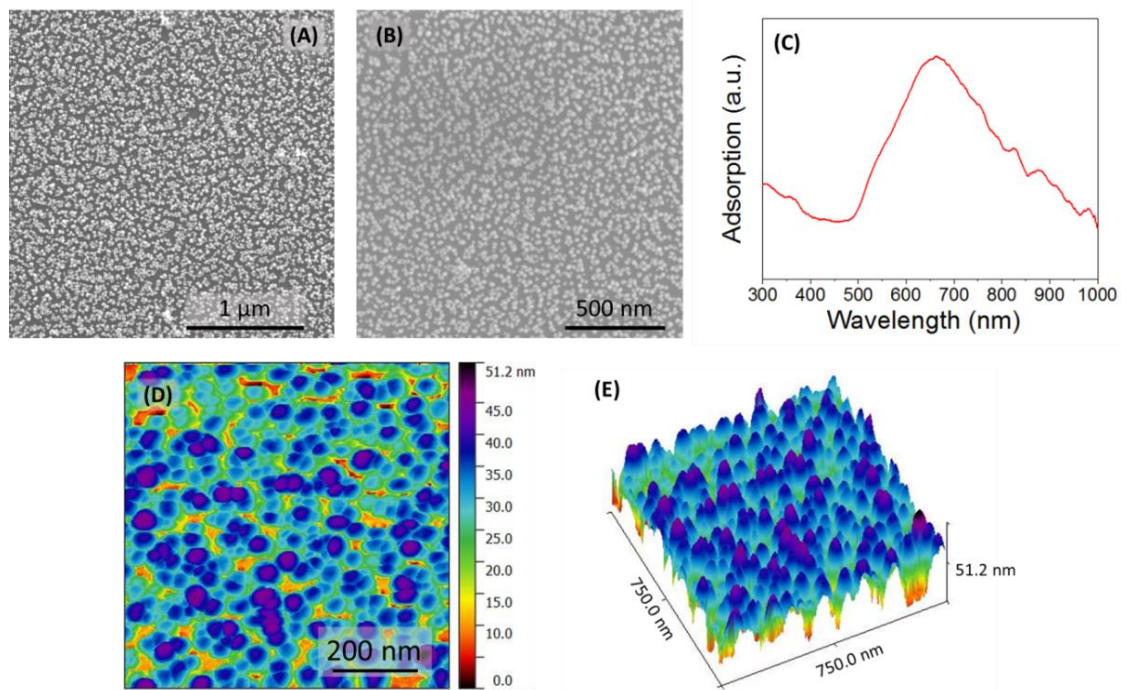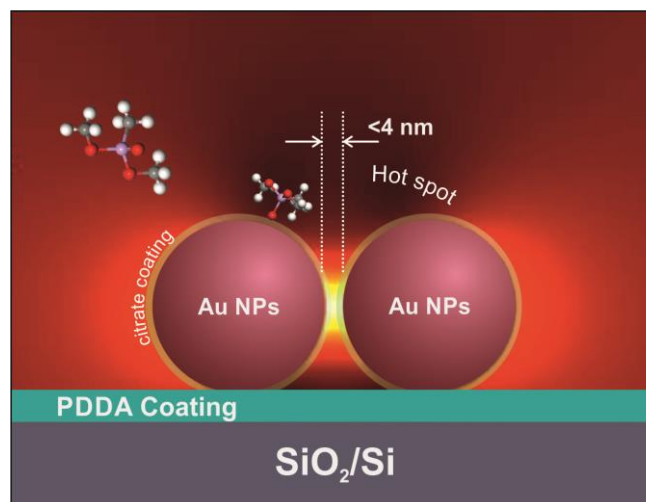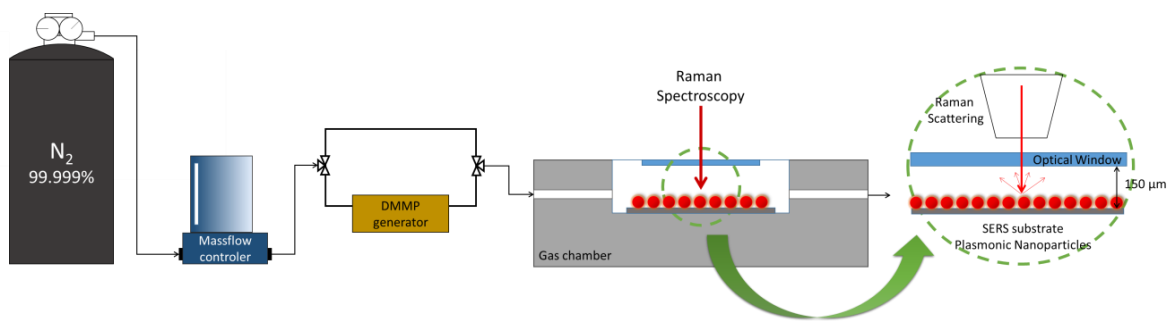
Experimental conditions: 0.033 MHz as detector horizontal shift. (B) Evolution of the SERS intensity attributed to the PC stretching peak of DMMP (centered at 715 cm^{-1}) with the DMMP concentration in the gas phase

Scheme 1. *Schematic diagram of SERS substrate and overview of the experimental set-up.*

Figure 1. *TEM images of Au@citrate NPs (A) and visualization of the citrate stabilizing layer (B). Statistical analysis of particle size from TEM images (C). Absorption spectrum of six independent synthesis batch of Au@citrate NPs (D); insert: Au@citrate solution in the UV cuvette.*
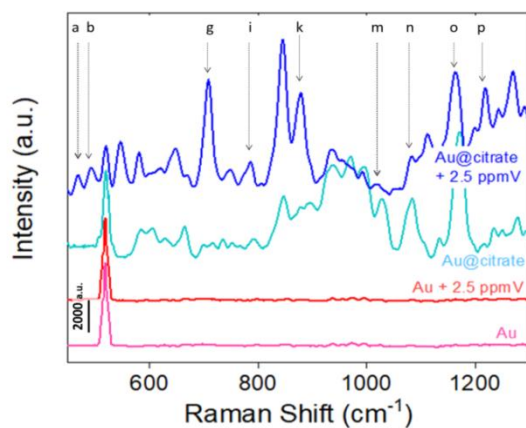
Figure 2. SEM images of high density Au@citrate monolayer onto SiO2/Si chips prepared by LbL assembly: (A) and (B). (C) Normalized UV-VIS spectrum of Au@citrate monolayer onto SiO2/Si chips. AFM characterization of high-density Au@citrate monolayer onto SiO2/Si chips: 2D (D) and 3D topography views (E).

Scheme 2. *Schematic representation of the surface structure of Au@citrate monolayer onto SiO₂/Si*

Figure 3. *Experimental set-up for SERS measurements in gas phase at ppmV level.*

Figure 4. *SERS spectra of high-density Au@citrate monolayers deposited on SiO2/Si chips during exposure to N2 (light blue) and to 2.5 ppmV DMMP gas (dark blue). Similar spectra have been recorded on O2 plasma treated samples: N2 (pink) and 2.5 ppmV DMMP gas N2 (red). Arrows point the main vibrational modes of DMMP (assignment described in Table 1).*
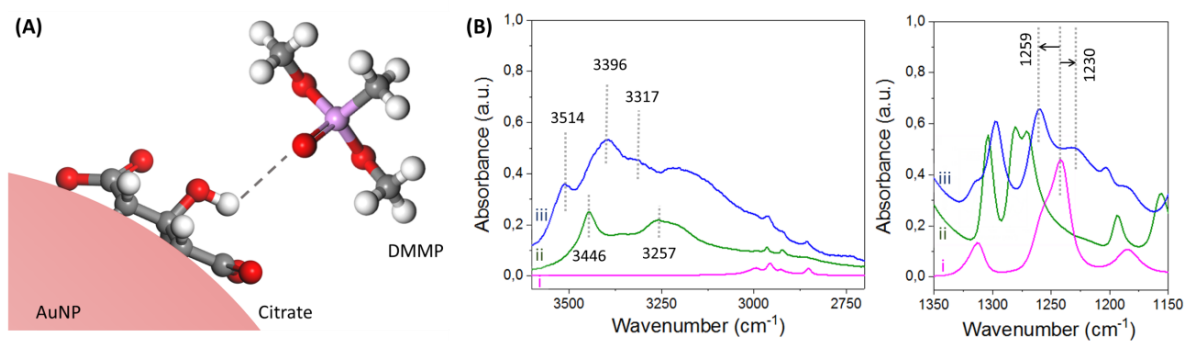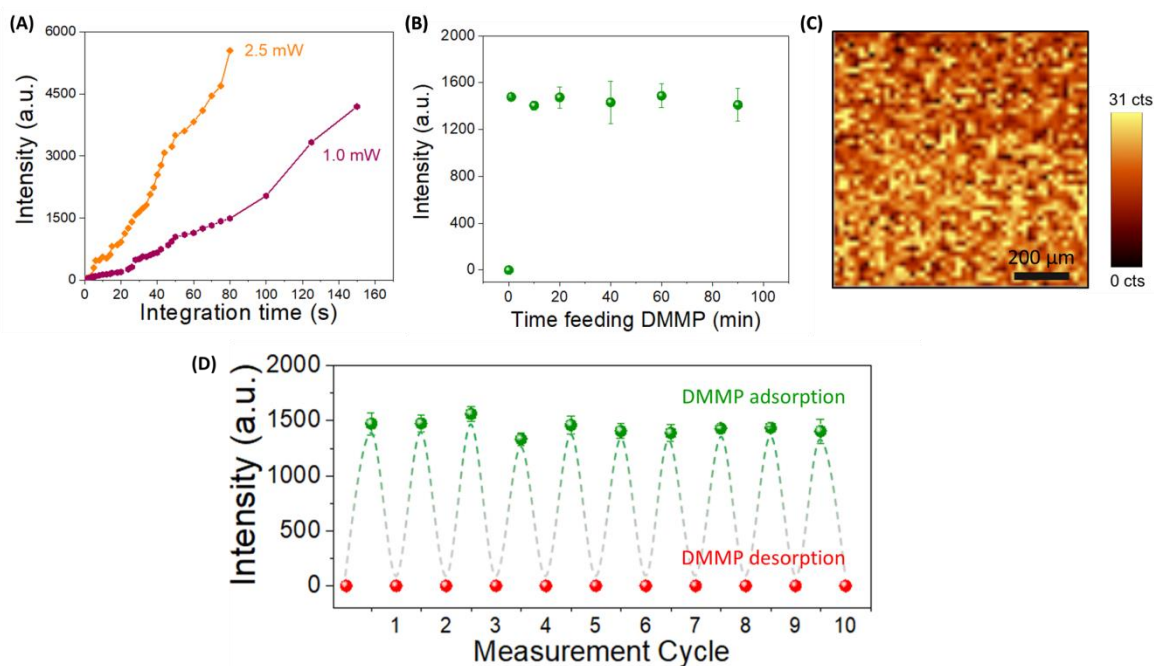
Figure 5. *(A) Formation of P-O---H-hydrogen bond interactions between the PO from DMMP and the citrate capping layer of Au NPs. (B) FTIR spectra at 3600-2700 cm^{-1} and 1350-1150 cm^{-1} of (i) DMMP liquid form, (ii) sodium citrate dihydrate salt, (iii) Au@citrate monolayers deposited on SiO$_2$/Si chips during upon saturation with DMMP molecules in vapor phase.*
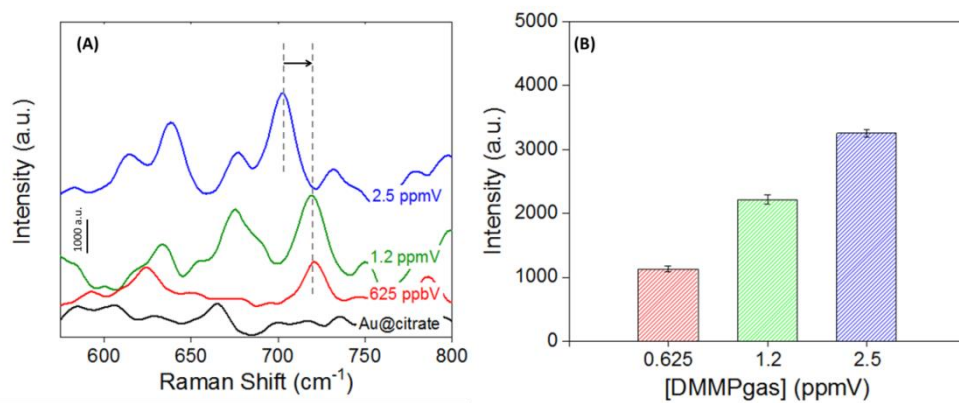
Table 1. *Tentative assignment of the experimental SERS bands for DMMP-Au@citrate species.*

Band	Band (cm^{-1})	Tentative Assignment	
a	467	DMMP	δ (P-O-CH$_3$)
b	492	DMMP	δ (PO$_3$)umbrella
c	519	Substrate	ν (Si-O-Si)
d	546	Citrate	δ (COO$^-$)
e	579	Citrate	δ (COO$^-$)
f	678	Citrate	δ (COO$^-$)
g	708	DMMP	ν(P-CH$_3$)+ν(P-O)+ δ (P-O-CH$_3$)
h	747	Citrate	ν (C-C)
i	788	DMMP	ν_{as}(O-P-O)
j	844	Citrate	ν_s (C-COO)
k	877	Citrate DMM	ν (C-COO) + δ (CH$_3$)
l	936	Citrate	ν (C-COO)
m	1028	DMMP and Citrate	ν (P=O) + ν (O-CH$_3$) ν_{as}(O-P-O) + δ (CH$_3$)
n	1081	DMMP and Citrate	ν_{as}(O-P-O) + ν (O-CH$_3$)
o	1162	Citrate DMM	δ (COO)+ δ (CH$_3$)
p	1220	DMMP	ν (P=O)+ δ (CH$_3$)
q	1268	Citrate	δ (COO)$^-$

δ = bending; ν = stretching;

Figure 6. *(A) SERS intensity of the Raman line at 718 cm^{-1} as a function of the power at the sample and the integration time in presence of 1.2 ppmV of DMMP in the gas phase. All the measurements were performed on the same chip. (B) SERS intensity values of the Raman lines at 718 cm^{-1} as a function of exposure time to 1.2 ppmV of DMMP in gas phase. All the measurements are performed on the same chip. (C) Raman mapping at 718 cm^{-1} across a 1x1 mm Au@citrate modified SiO$_2$/Si chip. Conditions: 2.5 mW, 1 s integration time, 1.2 ppmV of DMMP in gas phase and 20 μm as pitch. (D) Evolution of SERS intensity of the Raman line at 718 cm^{-}signal on the SERS substrate exposed to consecutive DMMP adsorption of 1.2 ppmV (green circle) and DMMP desorption in pure N$_2$ (red circle) cycles.*

Figure 7. *(A) SERS spectra of high-density Au@citrate monolayers onto SiO$_2$/Si chips during exposure to pure N$_2$ and 625 ppbV, 1.2 ppmV and 2.5 ppmV DMMP in gas. Experimental conditions: 0.033 MHz as detector horizontal shift. (B) Evolution of the SERS intensity attributed to the PC stretching peak of DMMP (centered at 715 cm^{-1}) with the DMMP concentration in the gas phase*

Graphical Abstract